Iranian Journal of Materials Forming

Research Article

The Effect of Simple Shear Extrusion on the Texture and Porosity Content of Al/Al₂O₃ Composites

M. Zabihi, F. Qods* and E. Emadoddin*

Faculty of Materials and Metallurgical Engineering, Semnan University, Semnan 35131-19111, Iran

ARTICLE INFO

ABSTRACT

In this study, aluminum/alumina composites with 1 and 3 vol% reinforcement particles were produced using powder metallurgy (PM); this was then followed by simple shear extrusion (SSE). Three SSE inserts with different distortion angles (α) were used in the SSE equipment. Three pressure values of 400, 600 and 800 MPa were selected for powder compression. Additionally, three different temperatures of 530, 550 and 570°C were chosen to evaluate the suitable sintering temperature and achieve the optimal SSE process. The effect of post-sintering annealing treatment on SSE feasibility was also investigated. In addition, porosity was measured by the Archimedes method and the microstructure of samples was evaluated using optical and scanning electron microscopy. Evaluation of the crystalline texture was examined by the X-ray method. It was found that the pressure of 800 MPa was the optimal value for the cold compression of powders and the temperature of 570°C was the best sintering temperature. It was also observed that the temperatures 400°C and 450°C had no effect on increasing the number of SSE passes. Porosity of the Al-3 vol% alumina sample was changed from 5.75% to 5.02% after three SSE passes with $\alpha = 10°$. A preferred crystallographic texture was not seen due to the amount of effective strain and the presence of micro-pores, but a very low intensity cube texture {001} <100> was seen in some regions.

1. Introduction

Particle reinforced aluminum matrix composites (AMCs) have unique and desirable thermal and mechanical properties such as light weight, high strength, and high elastic modulus. They are also relatively accessible and inexpensive, as compared to their continuous fiber and lamellar reinforced peers; they can be manufactured by both conventional and new techniques. In addition, discontinuously reinforced AMCs containing particulates are particularly interesting to the industrial community due to their isotropic behavior [1, 2]. Aluminum/alumina composites offer considerable potentials for wear resistance and high temperature applications in aerospace and aviation industries [3, 4]. There are different methods for manufacturing aluminum/alumina composites; including powder metallurgy (PM) [5], compo-casting [6], squeeze or stir casting [7], spray forming [8] and severe plastic deformation (SPD) [9].

The PM method is one of the most interesting ways due to several reasons. It offers some advantages not found in ingot melting or diffusion welding. The most significant feature is the low producing temperature, which prevents strong interfacial reactions, decreases undesirable alumina/aluminum reactions and also, ensures the uniform distribution of reinforcement particle powders in the matrix, in comparison with other AMC production techniques [10, 11].

An interesting topic over the last decade has been the introduction of SPD as a new way to manufacture ultra-fine-grained (UFG) materials by applying a large strain onto the materials [12]. One of the recent and attractive SPD procedures is simple shear extrusion (SSE), as presented by Pardis and Ebrahimi [13]. By passing the material through the deformation channel, increased shear strain could be exerted on the sample in a gradual manner [9]. The maximum shear effective strain is imposed at the middle plane with a maximum distortion angle and parallelogram shape. At the second half of the SSE channel, the distortion angle (α) is gradually decreased until it becomes zero. It is possible to produce a more homogeneous material by passing the 90° rotated samples in each consecutive cycle; this is done by using the sequential clockwise rotation as the route C [14].

The advantages of using SPD on porous composites include the formation of the demanded shape, control of porosity, matrix work hardening, noticeable improvements in properties, unusual microstructure, and development of complicated shapes [15].

Zabihi et al. [16] investigated the improvement of the mechanical properties of aluminum/alumina composite samples manufactured via powder metallurgy and this was followed by SSE. Hardness, ultimate shear strength and shear yield strength of the SSE-ed pure aluminum and aluminum/alumina composites were found to increase because of an increase in the number of SSE passes and distortion angles.

However, no investigation has yet focused on the simple shear extrusion capability at different compression and sintering conditions; also, different annealing temperatures and the crystalline texture of powdered Al/alumina composites should be evaluated. In this study, therefore, aluminum and alumina powder particles were mixed under argon atmosphere and then sintered at vacuum furnace. Different conditions for the preparation of the samples were examined to achieve the best conditions for the SSE operations. Finally, the texture evaluation of the SSE-ed samples was done.

2. Experimental Procedure

2.1. Materials

Received commercial aluminum powder with ~95% purity and particle size < 30 μm, as well as alumina powder with the size of 2-11 μm and polyhedral shape were utilized. The chemical composition of aluminum powders is shown in Table 1. Alumina powders specifications are also given in Table 2.

2.2. Milling process

Aluminum powders were mixed with 1 and 3 vol% of Al₂O₃ in a rotary-vibratory high energy planetary ball mill running at 110 rpm for 30 min. In this process, 20 balls composed of cold work tool steel with different sizes (3-10 mm in diameter) and 58-62 HRC hardness were used. The weight ratio of balls to powders was 8:1.

Table 1. Chemical composition of aluminum powders according to energy dispersive spectroscopy analysis

Element	Line	Intensity (c/s)	Error 2-sig	Conclusion	Units	KV 20.0 Take off Angle 35.0°
Al	Kα	950.20	5.513	94.690	wt.%	
P	Kα	4.33	0.981	0.550	wt.%	
Ag	Lα	7.12	0.788	3.754	wt.%	
Te	Lα	2.21	0.553	1.006	wt.%	
				100.000	wt.%	Total

Table 2. Characteristics of alumina powders particles as the reinforcement material [9]

Average particle size (μm)	Type of crystal	Melting point (°C)	Young's modulus (GPa)	Density (g cm⁻³)	Heat conductivity (W m⁻¹ k⁻¹)	Mohs-hardness	Thermal coefficient of expansion (10⁻⁶k⁻¹)
2-11	Hexagonal	2050	410	3.9	25	6.5	8.3

Stearic acid [17] was used as a process control agent (PCA) with a proportion of 1 wt.% of the total powders.

2.3. Compression and vacuum sintering process

Pure aluminum powders were prepared for comparison with other samples. These samples were pressed at the ultimate pressure of 400, 600, and 800 MPa in a hardened 1.2080 steel die with the interior space of $11\times11\times45$ mm^3 at room temperature. Manometer equipment was set up at the ram of the press to accurately measure the amount of applied pressure. Sprayed diluted graphite emulsion was used as a lubricating material for the die walls and the bottom of the punch. Prior to sintering, mixed powder particles were degassed in a vacuum resistance furnace in order to decrease the residual stresses and strain hardening which would lead to an increase in the compactability of the powders. The compressed powders were then vacuum sintered at 530°C, 550°C and 570°C for 90 min under vacuum condition (at 0.000004 mbar). The samples were gradually air-cooled.

2.4. Samples preparation

After sintering, the samples were cut perpendicular to the compression axis by a wire-cut machine; this was followed by grinding and polishing. All samples reached the final dimensions of 10 mm×10 mm in cross section and 40 mm in height.

2.5. Annealing before the SSE process

The annealing treatment was performed on the sintered parts at 400°C and 450°C for 30 min to achieve a better condition for the formability of the samples before the SSE process. Annealing is a heat treatment process that results in a softer or more relaxed state in the worked materials.

2.6. Simple shear extrusion (SSE)

The SSE process was done by a hydraulic control drive press with a capacity of 160 tons and ram speed of 0.5 mm/s at room temperature. This process was continued until the samples were cracked or fractured. Schematic view of the SSE procedure, done in the one step, as represented in Fig. 1(a) and 1(b), shows the SSE

die with distortion angle $(\alpha) = 8°$. A thin layer of teflon tape was used as the lubricating material between the specimens and the die. Bisection SSE-dies had a channel distortion angle with $\alpha_{max} = 22.5°$, $10°$, $8°$, and $\beta_{max} = 5.1°$. The equivalent strains enforced by the SSE dies are shown in Table 3.

Effective (ε_{eff}) and shear strains (γ) were calculated according to the analysis of other researchers. Pardis et al. [13] introduced a relation between the shear strain, effective strain and distortion angle based on the von-Mises criterion. Their findings can be summarized as follows:

$$\gamma = 2\tan\alpha \qquad (1)$$

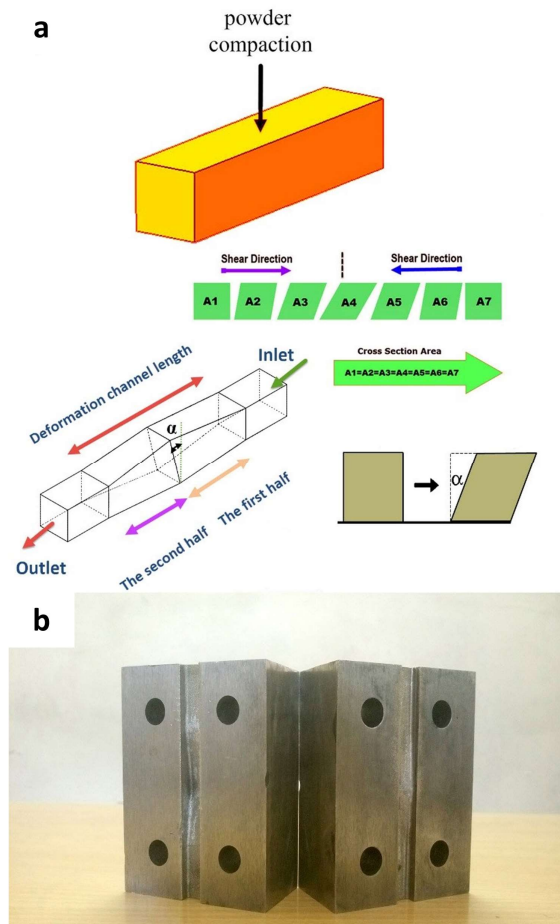$$\varepsilon_{eff} = \frac{\gamma}{\sqrt{3}} \qquad (2)$$

Fig. 1. (a) Schematic view of the SSE process, and (b) SSE die inserts with $\alpha = 8°$.

Table 3. SSE strains per pass of different dies applied on the samples

Distortion angles (°)	γ	ε_{eff}
$\alpha = 8$	0.281	0.1622
$\alpha = 10$	0.353	0.2038
$\alpha = 22.5$	0.829	0.4786

2.7. Quantitative texture evaluation

Powdered metal-matrix composites can be modified by the heavy plastic deformation process. It was expected that the process of deformation would lead to an uncommon increase of the strength behavior of the composite, and this would be accompanied by the particular changes of the metallic matrix textures. Texture measurements were then applied to characterize the orientation distribution of the crystalline grains in polycrystalline samples. XRD techniques are based on the elastic scattering of X-rays from structures that have a long-range order. One way to calculate the orientation distribution function (ODF) of a polycrystalline material is directly using the X-ray diffraction spectra. The X-ray source and the detector were oriented so that a specific value of 2θ would be determined. This procedure could make the measurement of the single Bragg reflection possible. The texture samples were provided by mechanical grinding and then polished to the final thickness of about 5 mm.

2.8. Porosity measurement

The experimental density of the specimens after vacuum sintering and SSE was estimated via the Archimedes method, according to the ISO 2738 standard [18]. The theoretical density was calculated by applying the mixture rule, based on the volume fraction of the matrix. Micro-porosities of the prepared samples were calculated from the difference between the anticipated and declared density. Porosity percentage of the samples was calculated by the following equation [16]:

$$P' = \left[1 - \frac{\rho_{mc}}{\rho_m\left(1 - V_p\right) + \rho_p V_p}\right] \times 100 \qquad (3)$$

where P' is the porosity percentage, ρ_{mc} is the measured density, ρ_m is the theoretical density of the material and V_p is the volume fraction of reinforcement.

3. Results and Discussion

3.1. SSE process

Material forming process involves plastic deformation, that leads to changes in both whole shape and cross-sectional area. However, while the manufacturing techniques of porous composites have been widely reported, there are limited studies on the severe plastic deformation of the composites. Although the pores may become smaller, they are not eliminated completely [19]. It is not, therefore, possible to precisely predict the deformation characteristics of porous composites, due to the inconsistency of the total volume caused by porosity closure [15].

To perform the SSE, the sintered parts pressed with the least pressure, 400 MPa, were first tested. Simultaneously, the three sintering temperatures mentioned earlier were considered and tested for this pressure.

Table 4 shows the SSE process feasibility information with the variables of compression pressures, sintering temperature, annealing temperatures before the process and distortion angles.

Table 4. Preparation conditions and SSE process feasibility

Applied pressure (MPa)	Sintering temperature (°C)				Descriptions
	530	550	570		
400	Failed	Failed	Failed		For all distortion angles
600	Failed	Failed	Failed		For all distortion angles
800	Failed	Failed	Failed	$\alpha = 22.5°$	
	2 Pass	2 Pass	3 Pass	$\alpha = 10°$	Without annealing treatment
	2 Pass	2 Pass	3 Pass	$\alpha = 8°$	
800	Failed	Failed	1 Pass with micro-cracks	$\alpha = 22.5°$	
	2 Pass	2 Pass	3 Pass	$\alpha = 10°$	With annealing treatment at 400°C and 450°C
	2 Pass	2 Pass	3 Pass	$\alpha = 8°$	

Shear strains were increased by increasing the α value in the die, whereas all samples with $\alpha = 22.5°$ and powder compression stresses less than 800 MPa were fractured without any successful passes. In addition, different annealing temperatures before the SSE process had no positive effect on the obtained results.

At the output of the die channel, in the pass with $\alpha = 22.5°$ and powder compression stresses less than 800 MPa, the cracking defect was first seen at the tips of the sample as well. This was because shear stresses and their distributions along the cross-section were the most important factors in the nucleation of edge cracks [20], as affected by the non-uniform deformation. It could be because of the inconvenient sample structure, such as micro-porosities and impurities, insufficient compression force and sintering temperature, and the effect of very fragile bond strength in some regions in cold compression when followed by the sintering process, as reported by some researchers [9, 16, 21]. With the increase of the sintering temperature, hardness and strength could also be increased due to the densification process [17].

3.2. Microstructural investigations

Fig. 2 illustrates the SEM images of the raw materials utilized in this study. Aluminum powders represented a wide size distribution of semi-spherical particles (Fig. 2(a)). Reinforcement powder particles also displayed irregular polyhedral particles with a narrow size distribution (Fig. 2(b)). As can be seen, Al_2O_3 powders showed a relatively high agglomeration.

Figs. 3(a) and 3(b), respectively exhibits the optical micrographs of pure Al and Al-3 vol% alumina metal matrix composites after being subjected to the vacuum sintering process. According to Fig. 3(a), micro-porosities could be observed in all areas of the matrix. Fig. 3(b) also represents the aluminum matrix containing coarse alumina particles, particle-free regions, and reinforcement coalescences. Selecting the appropriate pressure for compressing powders (800 MPa) and the modified temperature for the vacuum sintering process could reduce the fine pores and improve the initial conditions for the mechanical work. Pressure values of 825 and 850 MPa were used to press the powders, but there was no change in the number of extrusion passes.
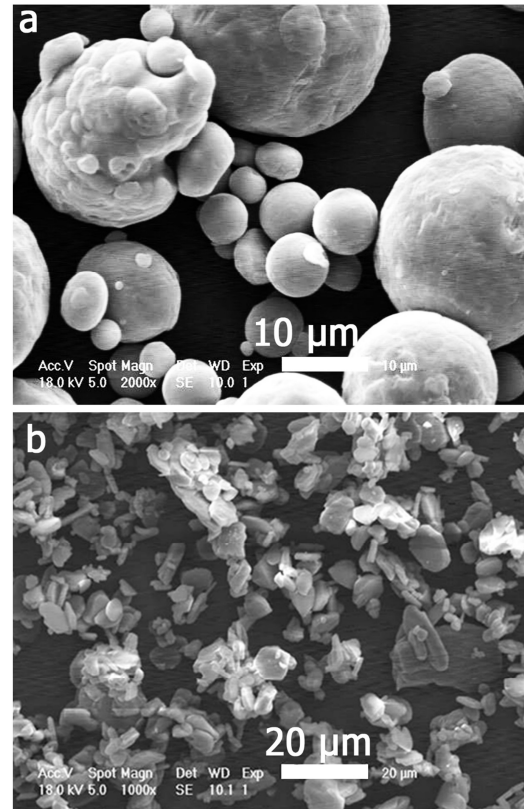

Fig. 2. SEM morphologies of raw materials: (a) Al powder and (b) alumina particles.
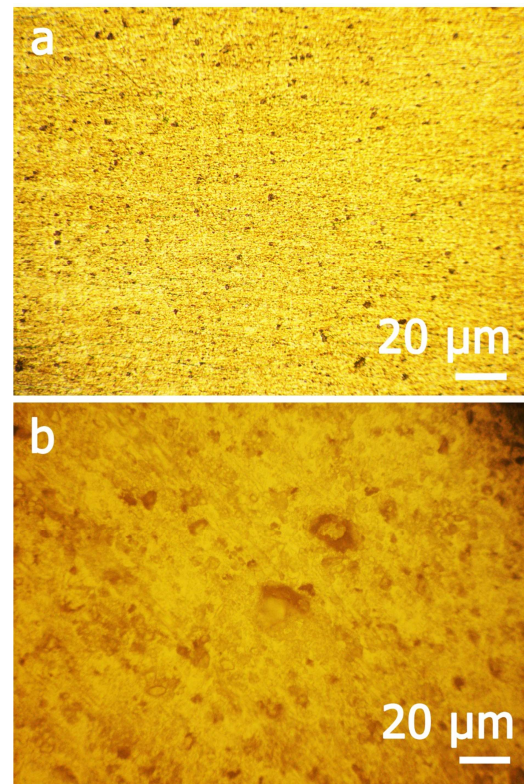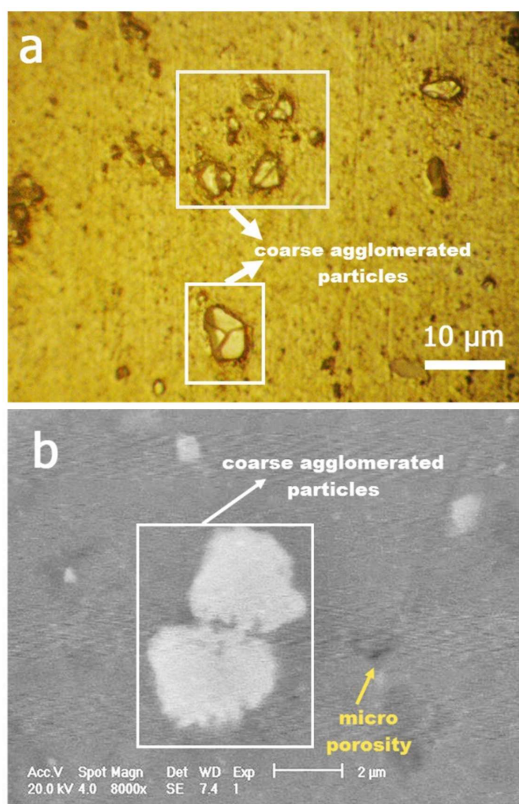

Fig. 3. Optical micrographs of (a) pure Al and (b) Al-3 vol% alumina after vacuum sintering.

The microstructure was not uniform, and in some areas, accumulation of reinforcing particles and micro-pores could be observed. Some previous studies [9, 22] have also shown that a sample free of porosity could not be produced unless the sintering temperature would be close to 600°C. However, the content of micro-pore coalescence is low, and the material has a good capability for mechanical working [21].

Figs. 4(a) and 4(b) demonstrate the optical and SEM micrographs of the side direction-transverse direction (SD-TD) plane of the SSE-ed Al-3 vol% alumina composite sample after three SSE passes. Before the first pass, the samples contained very coarse alumina particles and large particle-free zones. As a result of the shear strain, the distribution of reinforcing particles in the matrix was changed during the SSE process. In addition, the percentage of residual porosities decreased in comparison to the sintering process. The SSE process closed the micro-pores and redistributed the coarse agglomerated particles in the microstructure [16, 17].

Fig. 4. Optical and SEM micrograph of the (SD-TD) plane of the SSE-ed Al-3 vol% alumina composite sample after three SSE passes.

3.3. Texture development

Orientation distribution function (ODF) can be achieved through evaluating a set of pole figures. Here, four planes were used to calculate the crystallographic texture in the aluminum matrix composites, whereas for each of the indices, the needed pole figure (PF) was extracted. This method could be used to calculate ODFs from experimental PFs. Since the X-ray diffraction peaks of {111} and {110} planes were fully overlapped, the planes of {200}, {220}, and {311} were picked out to measure their complete PFs. Texture measurements were considered in the square cross section of the specimens in the plane perpendicular to the extrusion force (transverse direction-side direction (TD-SD)). The ODFs were presented as φ_2 constant sections.

Pole figures and inverse pole figures of the pure aluminum with different SSE conditions were obtained from the XRD analysis, as presented in Fig. 5. The plastic deformation of pure aluminum for which effective shear strain value of ~ 0.61 was applied could be seen in Fig. 5(a); the value of ~ 0.47 is shown in Fig. 5(b). The amount of porosity percentage, as shown in Fig. 5(a), was 4.7%; meanwhile, according to Fig. 5(b), it was calculated to be 4.84%. On the other hand, contour lines showed a very concise shear texture with a {100}<011> component, as well as a very low intensity cube texture {001}<100>, as could be observed in some regions. With respect to anisotropy in the structure, <100> direction had the highest density, while the <111> direction had the lowest one, regardless of porosities; they were reduced by increasing the porosity content.

A preferred crystallographic texture was not observed due to the amount of effective strain, the presence of micro-porosities and structural integrity [23-25]. As can be seen, there was no dominant texture after one and three passes for the composite sample. The linear contours of the ODF images for the composite samples were similar to that of the pure aluminum.

For a more accurate comparison of the texture changes during the SSE process, an Al-3 vol% alumina composite sample was used and PFs were prepared for passes 1 and 3 with the distortion angle of 10°, as presented in Fig. 6.
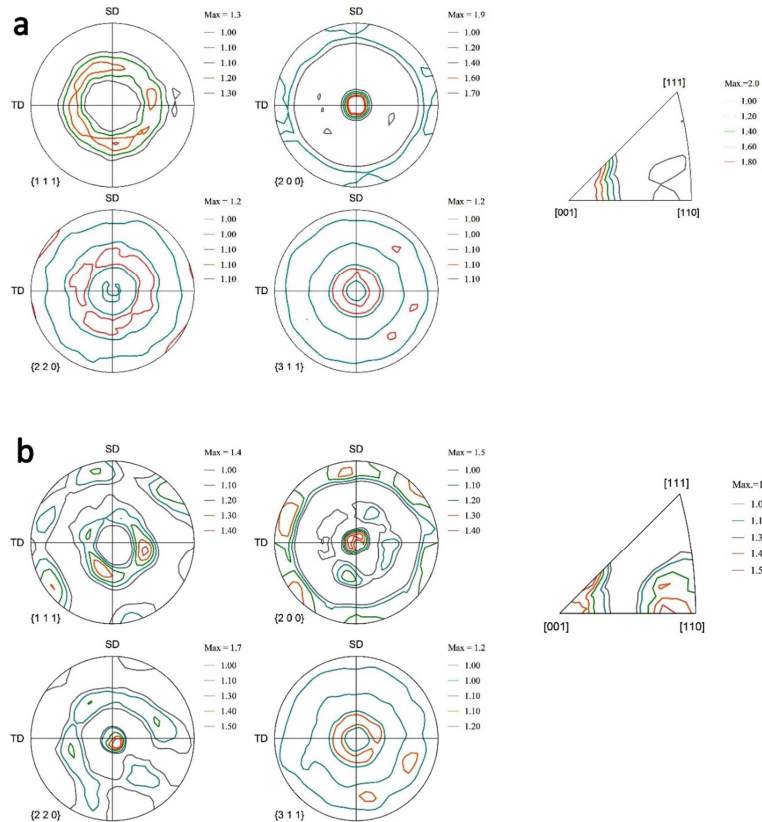
Fig. 5. Pole figures and inverse pole figure of pure aluminum with (a) $\alpha = 10°$ (3 passes), and (b) $\alpha = 22.5°$ (1 pass).
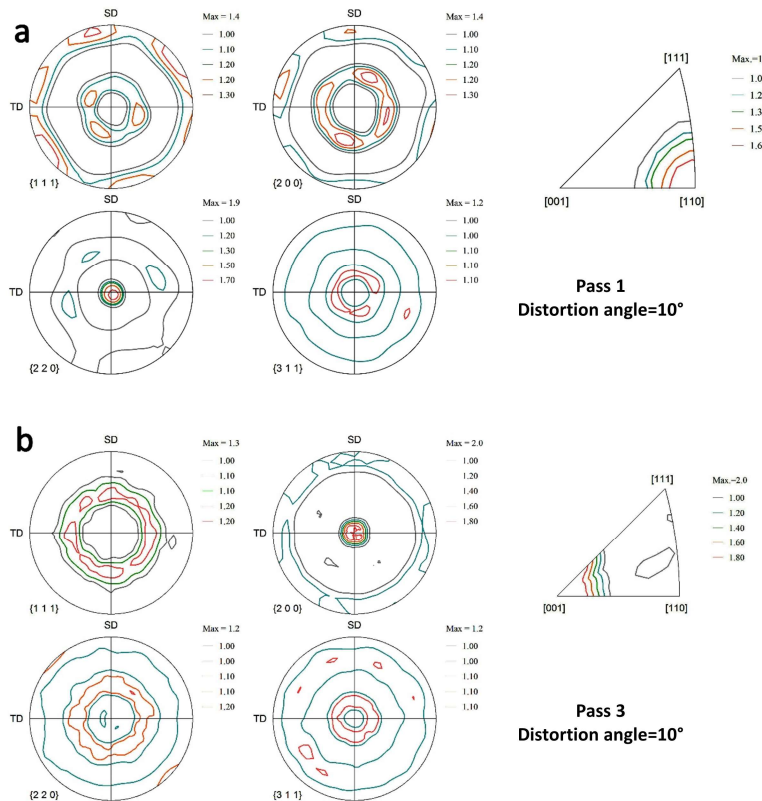

Fig. 6. Pole figures and inverse pole figure of Al-3 vol% alumina with $\alpha = 10°$ (a) 1 pass, and (b) 3 passes.

Figs. 7(a) and 7(b) show the ODF plots of the experimental texture for Al-3 vol% alumina with 1 pass and 3 pass samples and $\alpha = 10°$. The diagram shows that the overall texture intensity was decreased for the 3 pass sample. The preferred orientations of simple shear deformation disappeared in opposite directions during other SSE passes. This could be attributed to a shear reversal and shear strains counteraction in further passes [26]. Fig. 7(c) illustrates the ODF plot of SSE-ed pure Al with 1 pass in a die with $\alpha = 10°$. The Texture component was slightly sharper, as compared to Fig. 7(a). Based on the plastic deformation of the ceramic particulate reinforced aluminum matrix composites [27-28], researchers have corroborated that the rotations within the deformation zones in AMCs are dependent on both strain and slip systems in the matrix. For the present composite, the alumina particles were much harder than aluminum powders; also, they had a rather relatively anisotropic shape. As deformation occurs, large alumina particles with porosities are also presumed to disturb the slip pattern in the matrix.

3.4. Porosity content

In addition to the mentioned factors, porosity percentage has a significant effect on the mechanical performance of aluminum/alumina powdered composites [9]. In fact, the existence of porosities in aluminum matrix composites manufactured by powder metallurgy process leads to lower mechanical properties. After vacuum sintering, the porosity of the samples decreased due to an increase in the SSE passes, resulting in the increase of the applied shear strain. Consequently, after using the die with a distortion angle of 10°, the porosity of pure aluminum changed from 5.2% to 4.7% after 3 passes; in addition, the porosity of the composite including 3% of reinforcement was changed from 5.75% to 5.02%. As could be observed, the amount of porosity increased with a rise in the amount of reinforcement particles. Furthermore, the increase of α angle and SSE passes led to higher strain; this was then followed by pore reduction [18]. Porosities in aluminum-based composites could act as the preferred cracking starting points and diffusion pathways for cracks. As the applied
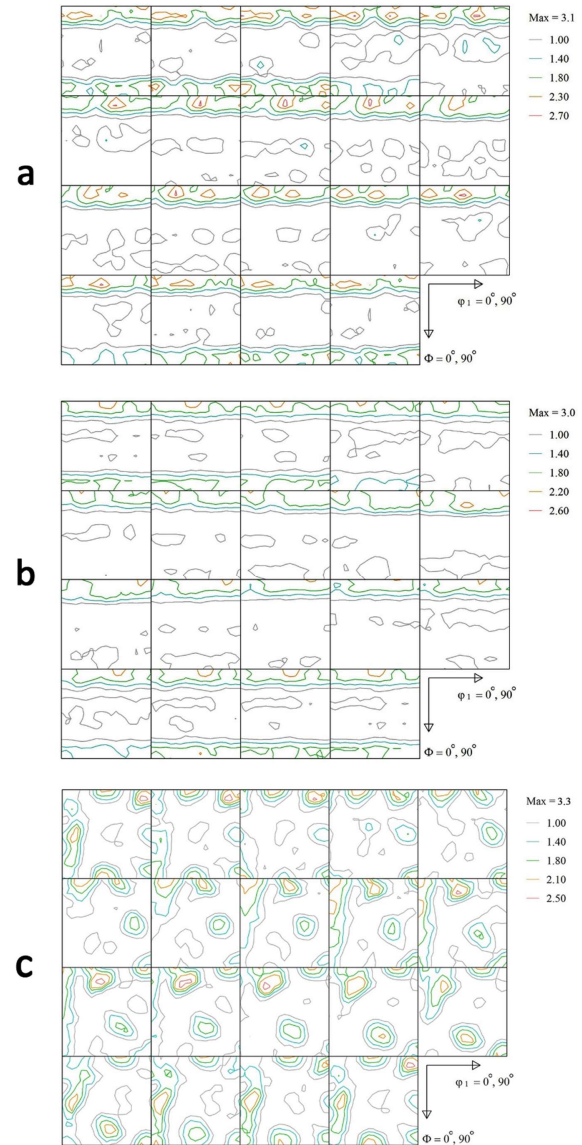

Fig. 7. ODF plots of the experimental texture for the Al-3 vol% alumina with (a) 1 pass, (b) 3 passes and (c) pure Al 1 pass samples with $\alpha = 10°$.

strain increased, the alumina powder particles were separated and the extrusion pressure rose; therefore, the pores were gradually closed [18, 29].

4. Conclusion

In this paper, Al/ 1 and 3 vol% alumina composites were manufactured by powder metallurgy, followed by the SSE process. The effects of cold compaction pressures, sintering temperatures, and post sintering annealing treatment on the SSE feasibility were then evaluated. In addition, porosity measurement and the

presence of possible texture were examined. Findings could be summarized as follows:

1. Among different pressure values for the cold compression of the powder, 800 MPa and the sintering temperature of 570°C were the optimal choices for applying the SSE process.

2. Annealing heat treatment after sintering on the samples at two different temperatures 400°C and 450°C had no effect on increasing the number of the SSE passes.

3. A preferred crystallographic texture was not seen due to the amount of effective strain and the presence of micro-pores. Contour lines illustrated a very concise shear texture with {100}<011> component; also, a lower intensity cube texture {001}<100> was seen in some regions.

4. At a constant shear strain, increasing the reinforcing particles reduced the texture intensity.

Acknowledgements

Conflict of Interests

The authors declare that they have no conflict of interest.

5. References

[1] C. Dhadsanadhep, T. Luangvaranunt, J. Umeda, K. Kondoh, Fabrication of Al/Al$_2$O$_3$ composite by powder metallurgy method from aluminum and rice husk ash, *Journal of Metals, Materials and Minerals*, 18(2) (2008) 99-102.

[2] M.J. Koczak, S.C. Khatri, J.E. Allison, M.G. Bader, in: S. Suresh, A. Mortensen, A. Needleman (Eds.), Fundamentals of metal matrix composites, Butterworth–Heinemann, Boston, 1993.

[3] K. Edalati, M. Ashida, Z. Horita, T. Matsui, H. Kato, Wear resistance and tribological features of pure aluminum and Al-Al$_2$O$_3$ composites consolidated by high-pressure torsion, *Wear*, 310(1-2) (2014) 83-89.

[4] A. Baradeswaran, A.E. Perumal, Study on mechanical and wear properties of Al 7075/Al$_2$O$_3$/graphite hybrid

composites, *Composites Part B: Engineering*, 56 (2014) 464-471.

[5] S. Pournaderi, S. Mahdavi, F. Akhlaghi, Fabrication of Al/Al$_2$O$_3$ composites by in-situ powder metallurgy (IPM), *Powder Technology*, 229 (2012) 276-284.

[6] B.C. Kandpal, J. kumar, H. Singh, Fabrication and characterisation of Al$_2$O$_3$/aluminium alloy 6061 composites fabricated by stir casting, *Materials Today: Proceedings*, 4(2) (2017) 2783-2792.

[7] X. Chang, G. Chen, W. Sun, H. Zhang, G. Chu, X. Zhang, F. Han, W. Zhang, Z. Du, Microstructures, mechanical properties and solidification mechanism of a hot tearing sensitive aluminum alloy asymmetric part fabricated by squeeze casting, *Journal of Alloys and Compounds*, 886 (2021) 161254.

[8] S.K. Chaudhury, C.S. Sivaramakrishnan, S.C. Panigrahi, A new spray forming technique for the preparation of aluminium rutile (TiO$_2$) ex situ particle composite, *Journal of Materials Processing Technology*, 145(3) (2004) 385-390.

[9] M. Zabihi, M.R. Toroghinejad, A. Shafyei, Application of powder metallurgy and hot rolling processes for manufacturing aluminum/alumina composite strips, *Materials Science and Engineering: A*, 560 (2013) 567-574.

[10] J.D. Torralba, C.E. Da Costa, F. Velasco, P/M aluminum matrix composites: an overview, *Journal of Materials Processing Technology*, 133(1-2) (2003) 203-206.

[11] R.K. Everett, R.J. Arsenault, Metal matrix composites: processing and interfaces, Academic Press, Elsevier, United States, 1991.

[12] R. Ebrahimi, A. Rezvani, E. Bagherpour, Circular simple shear extrusion as an alternative for simple shear extrusion technique for producing bulk nanostructured materials, *Procedia Manufacturing*, 15 (2018) 1502-1508.

[13] N. Pardis, R. Ebrahimi, Deformation behavior in simple shear extrusion (SSE) as a new severe plastic deformation technique, *Materials Science and Engineering: A*, 527(1-2) (2009) 355-360.

[14] E. Bagherpour, F. Qods, R. Ebrahimi, H. Miyamoto, Microstructure evolution of pure copper during a single pass of simple shear extrusion (SSE): role of shear reversal, *Materials Science and Engineering: A*, 666 (2016) 324-338.

[15] H. Utsunomiya, R. Matsumoto, Deformation processes of porous metals and metallic foams, *Procedia Materials Science*, 4 (2014) 245 -249.

[16] M. Zabihi, E. Emadoddin, F. Qods, Processing of Al/Al$_2$O$_3$ composite using simple shear extrusion (SSE) manufactured by powder metallurgy (PM), *Metals and Materials International*, 26(1), (2020) 1-13.

[17] M. Zabihi, M.R. Toroghinejad, A. Shafyei, Shear punch test in Al/alumina composite strips produced by powder metallurgy and accumulative roll bonding, *Materials Science and Engineering: A*, 667 (2016) 383-390.

[18] S. Amirkhanlou, R. Jamaati, B. Niroumand, M.R. Toroghinejad, Fabrication and characterization of Al/SiCₚ composites by CAR process, *Materials Science and Engineering: A*, 528(13-14) (2011) 4462-4467.

[19] A. Hassani, E. Bagherpour, F. Qods, Influence of pores on workability of porous Al/SiC composites fabricated through powder metallurgy+ mechanical alloying, *Journal of Alloys and Compounds*, 591 (2014) 132-142.

[20] N. Bayat Tork, N. Pardis, R. Ebrahimi, Investigation on the feasibility of room temperature plastic deformation of pure magnesium by simple shear extrusion process, *Materials Science and Engineering: A*, 560 (2013) 34-39.

[21] F.V. Lenel, Powder metallurgy: principles and applications, Metal Powder Industries Federation, Princeton, NJ, 1980.

[22] F. Bedir, B. Ogel. In: 3. Uluslarası toz metalurjisi kongresi (Ankara, Turkey, Gazi University, 2002), p. 4.

[23] H.J. Bunge, Texture analysis in materials science, Butterworths, London, UK, 1982.

[24] T. Eschner, J.J. Fundenberger, Application of anisotropic texture components, *Texture and Microstructures*, 28(3-4) (1997) 181-195.

[25] S.R. Kalidindi, C.A. Bronkhorst, L. Anand, Crystallographic texture evolution during bulk deformation processing of FCC metals, *Journal of the Mechanics and Physics of Solids*, 40(3) (1992) 537-569.

[26] H. Sheikh, R. Ebrahimi, E. Bagherpour, Crystal plasticity finite element modeling of crystallographic textures in simple shear extrusion (SSE) process, *Materials & Design*, 109 (2016) 289-299.

[27] F.J. Humphreys, The thermo mechanical processing of Al/SiC particulate composites, *Materials Science and Engineering: A*, 135 (1991) 267-273.

[28] F.J. Humphreys, W.S. Miller, M.R. Djazeb, Microstructural development during thermomechanical processing of particulate metal matrix composites, *Materials Science and Technology*, 6(11) (1990) 1157-1166.

[29] R. Jamaati, S. Amirkhanlou, M.R. Toroghinejad, B. Niroumand, Effect of particle size on microstructure and mechanical properties of composites produced by ARB process, *Materials Science and Engineering: A*, 528(4-5) (2011) 2143-2148.